

Heteroleptic dmit nickel complexes with bis(diphenylphosphanyl)amine ligands as robust molecular electrocatalysts for hydrogen evolution

Tao Li^{1,2} | Bin Xie^{1,3}  | Jia-Xi Cao⁴ | Dong-Liang Zhang² | Chuan Lai⁵ | Hua-Jun Fan² | Bin Zhao² | Wen-Yu Mou⁴ | Xiao-Xue Bai¹

¹School of Materials Science and Engineering, Sichuan University of Science and Engineering, Zigong, China

²School of Chemical Engineering, Sichuan University of Science and Engineering, Zigong, China

³Sichuan Province Key Laboratory of Comprehensive Utilization of Vanadium and Titanium Resources, Panzhihua University, Panzhihua, China

⁴College of Chemistry and Environmental Engineering, Sichuan University of Science and Engineering, Zigong, China

⁵School of Chemistry and Chemical Engineering, Sichuan University of Arts and Science, Dazhou, China

Correspondence

Bin Xie, School of Materials Science and Engineering, Sichuan University of Science and Engineering, Zigong 643000, China.

Email: xiebinqh@sina.com.cn

Chuan Lai, School of Chemistry and Chemical Engineering, Sichuan University of Arts and Science, Dazhou 635000, China.

Email: 20150002@sasu.edu.cn

Funding information

Graduate Innovation Fund Project of Sichuan University of Science and Technology, Grant/Award Numbers: y2019031, y2019023; Training Program of Innovation and Entrepreneurship for Undergraduates of Sichuan University of Science and Technology, Grant/Award Number: cx2019198; Science and Technology Bureau of Zigong City, Grant/Award Numbers: 2020MZGC06, 2019CXMZ01, 2015HX18; Open Fund

Four new neutral heteroleptic dmit nickel complexes bearing bis(diphenylphosphanyl)amine ligands, [RN (PPh₂)₂Ni(dmit)] (where dmit²⁻ = 1,3-dithiole-2-thione-4,5-dithiolate; R = (CH₂)₄CH₃ [**1**], (CH₂)₃OCH₃ [**2**], (CH₂)₂CH (CH₃)₂ [**3**], and CHPhCH₃ [**4**]), have been synthesized in moderated yields by the reactions between (*n*-Bu)₂Sn(dmit) and RN (PPh₂)₂NiCl₂ at room temperature. The complexes were fully characterized by elemental analysis, spectroscopy (Fourier transform infrared [FTIR], ultraviolet–visible [UV–vis], ¹H, ¹³C{¹H}, and ³¹P{¹H} nuclear magnetic resonance [NMR]), thermogravimetric analysis, and single crystal X-ray diffraction. In the crystal structures of **1–3** and **4**·2CH₂Cl₂, every nickel atom adopts a slightly distorted square-planar coordination by two phosphorus atoms of the RN (PPh₂)₂ ligand and two sulfur atoms of the dmit ligand. Furthermore, the electrochemical behaviors and electrocatalytic activities of **1–4** for hydrogen evolution have also been investigated by the cyclic voltammetry using trifluoroacetic acid (TFA) as the proton source. With the addition of 120-mM trifluoroacetic acid to 0.5-mM **1–4** in MeCN, the turnover frequency values of these catalysts were estimated to be 2827–5149 s⁻¹, and the relevant overpotentials were 0.72–0.79 V. Density functional theory (DFT) calculations and electrochemical investigations suggest that H₂ production proceeds via a key hydride intermediate [NiH (SH)] with an adjacent protonated sulfur atom of the dmit ligand in which the chelating sulfur atoms serve as proton relays. These findings demonstrate that these heteroleptic dmit nickel complexes could serve as robust and effective molecular electrocatalysts for hydrogen evolution.

KEYWORDS

bis(diphenylphosphanyl)amine, dmit²⁻, electrochemistry, hydrogen evolution, nickel complex

Project of Sichuan Province Key
Laboratory of Comprehensive Utilization
of Vanadium & Titanium Resources,
Grant/Award Number: 2018FTSZ09

1 | INTRODUCTION

With the consumption of fossil fuels, such as oil and natural gas, the society is facing increasingly serious problems about energy crisis and environmental pollution.^[1,2] Thus, one of the most attractive strategies to solve the current issues of environmental pollution and energy shortage is to develop clean and sustainable energy. In this respect, the focus has been increasingly placed on hydrogen (H₂) as an environmentally benign energy carrier.^[3,4] Hydrogen has many advantages over the traditional fossil fuels such as the highest specific combustion enthalpy of any chemical fuel, only water as the product, and not limited by Carnot cycle when used in a fuel cell.^[5] It could not only alleviate the energy crisis but also eliminate the environmental pollution caused by the fossil fuels. The precious metal platinum has been used as catalysts for hydrogen evolution,^[6] which has low overpotentials for the reduction of protons to hydrogen.^[5] However, the high cost of platinum is its biggest drawback.^[7–9] Research has been focused on developing highly efficient and robust hydrogen evolution catalysts with earth-abundant metal^[6–8] such as iron,^[10–14] cobalt,^[8,15–20] manganese,^[9,21] copper,^[20,22–24] and molybdenum^[25–27] complexes. Among them, metal nickel stands out because (1) it resides in the same group as Pt but on the first row of transition metals, and (2) it is an earth-abundant metal for hydrogen production.^[28] Many heteroleptic nickel complexes with diphosphine ligands have been extensively explored as catalysts for hydrogen evolution.^[28–32] The dithiolene ligand is usually introduced in the Ni complex as proton relays and protonation sites.^[7,17] Recently, Gan and coworkers reported that a bioinspired complex, [(dppf)Ni(bdt)], can catalyze protons reduction to hydrogen with a turnover frequency (TOF) of 1240 s⁻¹ and an overpotential requirement of 265 mV at the low HOAc concentrations.^[33,34] Similar electrocatalyst [(dppp)Ni(pdt)] demonstrated high-efficient hydrogen evolution but was unstable and degraded into an electrode-adsorbed film under the reducing and protic conditions.^[35] Notably, bis(diphenylphosphanyl)amine (RN (PPh₂)₂) revealed as an excellent diphosphine ligand whose structure is close to bis(diphenylphosphanyl)methane (dppm) but having other advantages than dppm.^[8] The RN (PPh₂)₂ metal complexes are excellent catalysts for hydrogen evolution, ethene oligomerization, and Suzuki–Miyaura reaction.^[32,36–39] However, little research on the

dithiolene/dithiolate nickel complexes with RN (PPh₂)₂ ligands as hydrogen evolution catalysts has been investigated.^[32,40]

1,3-Dithiole-2-thione-4,5-dithiolate (dmit²⁻) is a conjugated, planar structured dithiolene ligand. This sulfur-rich heterocyclic ligand has strong affinities binding to metal ions and demonstrates reversible redox properties.^[41] In recent years, a considerable amount of interest has been placed on this dmit complexes^[41–46] and their applications in organic conductors,^[41,47,48] chemical sensors,^[49,50] magnetic materials,^[42,43] and nonlinear optical materials.^[44,49,51–53] As an analogous to dmit, the maleonitriledithiolate (mnt²⁻) complexes also attracted some attentions for the prominent biomimetic and redox properties.^[54] A homoleptic complex (n-Bu₄N) [Co(mnt)₂] was first reported to have excellent photo- and electrocatalytic activities for the reduction of protons to hydrogen.^[54,55] And an electrochemical–chemical–electrochemical–chemical mechanism (ECEC) involving the protonation of two sulfur atoms in different mnt ligands was proposed.^[56] (n-Bu₄N)[Ni(mnt)₂] has also been reported to homogeneously electrocatalyze the reduction of protons to hydrogen.^[57] Study showed that the diprotonation occurs at two sulfur atoms from different mnt ligands with a distorted nickel hydride intermediate. In addition, the homoleptic complexes of [BzPyN(CH₃)₂]₂[Ni(mnt)₂] and [4-ClBzPyN(CH₃)₂]₂[Ni(mnt)₂] with different nickel oxidation states can also electrocatalyze protons reduction with the ECEC mechanism.^[58] However, the protonation occurs at nickel center, which suggest that the nickel (III) complex is the better catalyst than the nickel (II) species.^[58] However, no nickel complexes containing dmit ligand, either homoleptic or heteroleptic, have been currently reported for electrocatalytic reduction of protons to hydrogen.

Inspired by the effective catalytic hydrogen evolution performances of the nickel complexes containing diphosphine and dithiolate ligands,^[28,29,32,33] and as a continuation of studies on the heteroleptic nickel complexes,^[46,58,59] we herein report the synthesis and structural characterization of four novel heteroleptic nickel complexes bearing RN (PPh₂)₂ and dmit ligands, [RN (PPh₂)₂Ni(dmit)] (R = (CH₂)₄CH₃ [1], (CH₂)₃OCH₃ [2], (CH₂)₂CH(CH₃)₂ [3], and CHPhCH₃ [4]). These complexes were characterized by elemental analysis, Fourier transform infrared (FTIR), ultraviolet–visible (UV–vis), ¹H, ¹³C{¹H}, and ³¹P{¹H}

nuclear magnetic resonance (NMR) spectroscopies. Their electrochemical properties were studied by cyclic voltammetry (CV), and their electrocatalytic performances for hydrogen production were investigated in the presence of trifluoroacetic acid (TFA) in MeCN. Density functional theory (DFT) computations provide further insights into their mechanisms for hydrogen evolution, and their stabilities for hydrogen evolution were also evaluated in the presence of concentrate TFA and under the electrocatalytic conditions.

2 | EXPERIMENTAL

2.1 | Materials and methods

All reactions and operations were carried out using standard Schlenk techniques under nitrogen atmosphere. Solvents were dried and distilled by using standard procedures. NiCl₂·6H₂O, Et₃N, Ph₂PCL, NH₂(CH₂)₃OCH₃, NH₂(CH₂)₄CH₃, NH₂(CH₂)₂CH(CH₃)₂, NH₂CHPhCH₃, CS₂, ZnCl₂, Et₄NBr, *n*-Bu₂SnCl₂, and sodium were obtained commercially and used as received. Ferrocene and *n*-Bu₄NPF₆ were bought from commercial and purified multiple times by crystallization before use, respectively. RN (PPh₂)₂, RN (PPh₂)₂NiCl₂, [NEt₄]₂[Zn (dmit)₂], and (*n*-Bu)₂Sn(dmit) were prepared according to the literature procedures.^[36,59–63] Preparative thin layer chromatography (TLC) was carried out on glass plates (26 × 20 × 0.25 cm³) coated with silica gel G. Melting points were measured on a WRS-2C microscopic melting point apparatus and were uncorrected. Elemental analyses were investigated on an Elementar Vario EL cube analyzer. FTIR spectra were conducted using a NICOLET 6700 infrared spectrophotometer with pressed KBr disk at room temperature. NMR spectra were obtained on a Bruker AV400 NMR spectrometer with CDCl₃ as solvent at room temperature. ¹H NMR (400 MHz) and ¹³C{¹H} NMR (101 MHz) spectra were referenced to residual solvent relative to tetramethyl-silane, and ³¹P{¹H} NMR (162 MHz) spectra were referenced to external 85% H₃PO₄. UV–vis absorption spectra in acetonitrile were measured using a TU-1950 UV–vis spectrophotometer with a 1-cm quartz cell at room temperature. Thermogravimetric analyses were recorded on a NETZSCH STA 409 PC/PG instrument under nitrogen atmosphere. CV measurements were performed on a CHI660E instrument equipped with a three-electrode cell, a 3-mm diameter glassy carbon working electrode, a platinum wire counter electrode, and a nonaqueous Ag/Ag⁺ reference electrode at room temperature. The supporting electrolyte was 0.1-M *n*-Bu₄NPF₆ in MeCN. The glassy

carbon electrode was polished with alumina (1 μm) on a polishing cloth before each measurement. The solution was purged with argon or nitrogen gas prior to measurements. At the end of each experiment, ferrocene was added as an internal standard. The potential scale was calibrated against the Fc⁺/Fc couple and reported versus this reference system, whose potential was measured in the cell at the end of each experiment. Catalysis studies for hydrogen evolution were carried out by sequential addition of TFA by syringe from solutions of the acid in the same electrolyte. Controlled potential electrolysis (CPE, namely, the bulk electrolysis) experiments were performed at −1.60 V versus Fc⁺/Fc using 0.5-mM complex **1** and 260-mM TFA in MeCN (40 mL) with 0.1-M *n*-Bu₄NPF₆ in an air-tight single compartment cell. The cell was sparged at least 15 min with nitrogen atmosphere before electrolysis and then electrolysis was allowed to run for 1.5 h. After electrolysis, a sample of the headspace was injected into a GC7980 gas chromatograph equipped with a thermal conductivity detector (TCD) to analyze the gas composition.

2.2 | Synthesis

2.2.1 | [CH₃(CH₂)₄N(PPh₂)₂Ni(dmit)] (1)

CH₃(CH₂)₄N(PPh₂)₂NiCl₂ (0.292 g, 0.5 mmol) in CH₂Cl₂ (10 mL) was slowly added to a solution of (*n*-Bu)₂Sn (dmit) (0.5 mmol, 0.215 g) in acetone (5 mL), and the mixture was stirred for 2 h at room temperature and resulted in a green solution. Solvents were removed under vacuum, and the residue was subjected to TLC separation using CH₂Cl₂ as eluent to give **1** as a green solid. Yield: 0.305 g, 86%. m.p. (°C): 240.0–240.5. Anal. Calc. (%) for C₃₂H₃₁NNiP₂S₅: C, 54.09; H, 4.40; N, 1.97; S, 22.56. Found (%): C, 54.34; H, 4.58; N, 1.79; S, 22.32. FTIR (KBr disk, cm⁻¹): ν_{C=C} 1436 (s), ν_{C-S} 1104 (s), ν_{C-S} 1053 (vs), ν_{P-N-P} 828 (s). ¹H NMR (400 MHz, CDCl₃, ppm): 0.59 (t, *J*_{HH} = 7.2 Hz, 3H, CH₃), 0.72–0.84, 0.85–0.97, and 1.03–1.11 (tm, 6H, NCH₂(CH₂)₃), 2.85–2.96 (m, 2H, NCH₂), 7.52 (t, *J*_{HH} = 7.4 Hz, 8H, *m*-PhH), 7.62 (t, *J*_{HH} = 7.4 Hz, 4H, *p*-PhH), 7.83 (dd, ³*J*_{PH} = 13.0 Hz, *J*_{HH} = 6.8 Hz, 8H, *o*-PhH). ¹³C{¹H} NMR (101 MHz, CDCl₃, ppm): 13.84 (s, CH₃), 21.99, 29.07, and 29.42 (3s, NCH₂(CH₂)₃), 48.86 (t, ²*J*_{PC} = 4.8 Hz, NCH₂), 129.30 (s, *p*-PhC), 129.57 (t, ³*J*_{PC} = 5.7 Hz, *m*-PhC), 129.78 (s, S₂C=CS₂), 133.10 (t, ²*J*_{PC} = 6.2 Hz, *o*-PhC), 138.81 (t, ¹*J*_{PC} = 11.1 Hz, *i*-PhC), 221.75 (s, S=C). ³¹P{¹H} NMR (162 MHz, CDCl₃, 85% H₃PO₄, ppm): 58.29 (s, NP₂). UV–vis (MeCN, λ_{max}, nm): 226, 241, 267, 310, 463.

2.2.2 | [CH₃O(CH₂)₃N(PPh₂)₂Ni(dmit)] (2)

Complex **2** was synthesized by a similar procedure as described for **1**, but it used CH₃O(CH₂)₃N(PPh₂)₂NiCl₂ (0.5 mmol, 0.293 g) instead of CH₃(CH₂)₄N(PPh₂)₂NiCl₂. Solvents were removed under vacuum, and the residue was subjected to TLC separation using CH₂Cl₂ as eluent to give **2** as a green solid. Yield: 0.299 g, 84%. m.p. (°C): 240.6–241.5. Anal. Calc. (%) for C₃₁H₂₉NNiOP₂S₅: C, 52.26; H, 4.10; N, 1.97; S, 22.50. Found (%): C, 52.51; H, 4.25; N, 1.76; S, 22.29. FTIR (KBr disk, cm⁻¹): ν_{C=C} 1434 (s), ν_{C-S} 1105 (vs), ν_{C=S} 1051 (vs), ν_{P-N-P} 829 (s). ¹H NMR (400 MHz, CDCl₃, ppm): 1.29–1.37 (m, 2H, NCH₂CH₂), 2.92 (t, *J*_{HH} = 5.7 Hz, 2H, NCH₂), 2.98–3.12 (m, 2H, OCH₂), 3.03 (s, 3H, OCH₃, overlaps with the oxomethylene group signal), 7.52 (t, *J*_{HH} = 7.4 Hz, 8H, *m*-PhH), 7.61 (t, *J*_{HH} = 7.4 Hz, 4H, *p*-PhH), 7.83 (dd, *J*_{PH} = 13.0 Hz, *J*_{HH} = 6.8 Hz, 8H, *o*-PhH). ¹³C{¹H} NMR (101 MHz, CDCl₃, ppm): 29.90 (s, NCH₂CH₂), 46.19 (t, ²*J*_{PC} = 4.7 Hz, NCH₂), 58.70 (s, OCH₃), 69.34 (s, OCH₂), 129.02 (s, *p*-PhC), 129.26 (s, S₂C=CS₂), 129.55 (t, ³*J*_{PC} = 5.7 Hz, *m*-PhC), 133.04 (t, ²*J*_{PC} = 6.1 Hz, *o*-PhC), 138.80 (t, ¹*J*_{PC} = 11.1 Hz, *i*-PhC), 221.50 (s, S=C). ³¹P{¹H} NMR (162 MHz, CDCl₃, 85% H₃PO₄, ppm): 58.56 (s, NP₂). UV-vis (MeCN, λ_{max}, nm): 227, 241, 266, 309, 463.

2.2.3 | [(CH₃)₂CH(CH₂)₂N(PPh₂)₂Ni(dmit)] (3)

Complex **3** was synthesized by a similar procedure as described for **1**, but it used (CH₃)₂CH(CH₂)₂N(PPh₂)₂NiCl₂ (0.292 g, 0.5 mmol) instead of CH₃(CH₂)₄N(PPh₂)₂NiCl₂. Solvents were removed under vacuum, and the residue was subjected to TLC separation using CH₂Cl₂ as eluent to give **3** as a green solid. Yield: 0.287 g, 81%. m.p. (°C): 268.1–269.8. Anal. Calc. (%) for C₃₂H₃₁NNiP₂S₅: C, 54.09; H, 4.40; N, 1.97; S, 22.56. Found (%): C, 54.47; H, 4.65; N, 1.88; S, 22.71. FTIR (KBr disk, cm⁻¹): ν_{C=C} 1433 (s), ν_{C-S} 1100 (s), ν_{C=S} 1050 (vs), ν_{P-N-P} 851 (s). ¹H NMR (400 MHz, CDCl₃, ppm): 0.53 (d, *J*_{HH} = 6.6 Hz, 6H, 2CH₃), 0.88–1.01 (m, 2H, NCH₂CH₂), 1.05–1.13 (m, 1H, (CH₃)₂CH), 2.83–2.99 (m, 2H, NCH₂), 7.53 (t, *J*_{HH} = 7.4 Hz, 8H, *m*-PhH), 7.62 (t, *J*_{HH} = 7.4 Hz, 4H, *p*-PhH), 7.83 (dd, *J*_{PH} = 13.0 Hz, *J*_{HH} = 6.8 Hz, 8H, *o*-PhH). ¹³C{¹H} NMR (101 MHz, CDCl₃, ppm): 22.21 (s, CH₃), 26.23 (s, NCH₂CH₂), 38.50 (s, (CH₃)₂CH), 47.20 (t, ²*J*_{PC} = 4.8 Hz, NCH₂), 129.28 (s, *p*-PhC), 129.58 (t, ³*J*_{PC} = 5.7 Hz, *m*-PhC), 129.77 (s, S₂C=CS₂), 133.10 (t, ²*J*_{PC} = 6.1 Hz, *o*-PhC), 138.80 (t, ¹*J*_{PC} = 11.1 Hz, *i*-PhC), 221.77 (s, S=C). ³¹P{¹H} NMR (162 MHz, CDCl₃, 85% H₃PO₄, ppm): 58.40 (s, NP₂). UV-vis (MeCN, λ_{max}, nm): 226, 242, 266, 310, 463.

2.2.4 | [CH₃CHPhN(PPh₂)₂Ni(dmit)] (4)

Complex **4** was synthesized by a similar procedure as described for **1**, but it used CH₃CHPhN(PPh₂)₂NiCl₂ (0.309 g, 0.5 mmol) instead of CH₃(CH₂)₄N(PPh₂)₂NiCl₂. Solvents were removed under vacuum, and the residue was subjected to TLC separation using CH₂Cl₂ as eluent to give **4** as a green solid. Yield: 0.271 g, 73%. m.p. (°C): 241.3–242.1. Anal. Calc. (%) for C₃₅H₂₉NNiP₂S₅: C, 56.46; H, 3.93; N, 1.88; S, 21.53. Found (%): C, 56.44; H, 4.15; N, 1.97; S, 21.32. FTIR (KBr disk, cm⁻¹): ν_{C=C} 1434 (s), ν_{C-S} 1097 (s), ν_{C=S} 1053 (vs), ν_{P-N-P} 889 (s). ¹H NMR (400 MHz, CDCl₃, ppm): 1.08 (d, *J*_{HH} = 7.1 Hz, 3H, CH₃), 4.52 (tq, *J*_{PH} = 13.9 Hz, *J*_{HH} = 7.0 Hz 1H, NCH), 6.62 (d, *J*_{HH} = 7.3 Hz, 2H, *o*-CHPhH), 6.93 (t, *J*_{HH} = 7.7 Hz, 2H, *m*-CHPhH), 7.08 (t, *J*_{HH} = 7.4 Hz, 1H, *p*-CHPhH), 7.47 (dt, *J*_{PH} = 15.0 Hz, *J*_{HH} = 7.5 Hz, 8H, *m*-PPhH), 7.52–7.64 (m, 4H, *p*-PPhH), 7.82 (dd, *J*_{PH} = 13.2 Hz, *J*_{HH} = 6.9 Hz, 4H, *o*-PPhH), 7.91 (dd, *J*_{PH} = 13.1 Hz, *J*_{HH} = 6.9 Hz, 4H, *o*-PPhH). ¹³C{¹H} NMR (101 MHz, CDCl₃, ppm): 22.01 (t, ³*J*_{PC} = 2.4 Hz, CH₃), 62.09 (t, ²*J*_{PC} = 4.7 Hz, NCH), 128.17 (s, *o*-CHPhC), 128.77 (s, *m*-CHPhC), 128.98 (s, *p*-CHPhC), 129.32 (t, ³*J*_{PH} = 5.9 Hz, *m*-PPhC), 132.87, 133.00 (2s, S₂C=CS₂), 133.27 (t, ⁴*J*_{PC} = 6.2 Hz, *p*-PPhC), 133.71 (t, ²*J*_{PC} = 6.1 Hz, *o*-PPhC), 138.81 (t, ¹*J*_{PC} = 10.7 Hz, *i*-PPhC), 139.26 (t, ³*J*_{PC} = 2.3 Hz, *i*-CHPhC), 221.42 (s, S=C). ³¹P{¹H} NMR (162 MHz, CDCl₃, 85% H₃PO₄, ppm): 62.10 (s, NP₂). UV-vis (MeCN, λ_{max}, nm): 227, 243, 266, 311, 465.

2.3 | X-ray crystal structure determinations

The single crystals of **1–3** and **4**·2CH₂Cl₂ suitable for X-ray diffraction analyses were grown by slow evaporation of the CH₂Cl₂/hexane solutions at about –10°C. The crystal data of **2** and **3** were collected on a charge-coupled device (CCD) diffractometer by using Mo-Kα radiation sealed X-ray tube (λ = 0.71073 Å) in the ω scanning mode at 293(2) K, and the crystal data for **1** and **4**·2CH₂Cl₂ were collected on a Supernova Dual with Atlas S2 diffractometer by using Cu-Kα radiation sealed X-ray tube (λ = 1.54184 Å) in ω scanning mode at 162.00(10) K. Using Olex2,^[64] the structures were solved by direct methods with the SIR2004 structure solution program^[65] and refined by full-matrix least-squares minimization with the SHELXTL refinement package^[66] on *F*². All non-hydrogen atoms were located from the Fourier maps and were refined anisotropically. All hydrogen atoms were refined isotropically, with the isotropic vibration parameters related to the non-hydrogen atom to which

they are bonded. Relevant crystallographic details are summarized in Table 1.

2.4 | Computational details

DFT calculations were used to model the mechanisms of the proton reduction reaction. All calculations were

carried out with the Gaussian 09 program.^[67] All geometries in this study were optimized using B3LYP functional^[68,69] in combination with the 6-311G (d, p) basis set.^[70] The DFT-D3 model was applied for the dispersion correction to accurately compute the London dispersion interactions. Separate frequency calculations were carried out to confirm the optimized geometry as local minima. The SMD solvation model was applied to simulate the

TABLE 1 Crystal data and structure refinements details for **1–3** and **4·2CH₂Cl₂**

Complex	1	2	3	4·2CH₂Cl₂
Empirical formula	C ₃₂ H ₃₁ NNiP ₂ S ₅	C ₃₁ H ₂₉ NNiOP ₂ S ₅	2(C ₃₂ H _{29,5} NNiP ₂ S ₅)	C ₃₅ H ₂₉ NNiP ₂ S ₅ ·2CH ₂ Cl ₂
Formula weight	710.53	712.50	1418.03	914.39
Temperature (K)	162.00(10)	293(2)	293(2)	162.00(10)
Radiation	Cu-K _α	Mo-K _α	Mo-K _α	Cu-K _α
Wavelength (Å)	1.54184	0.71073	0.71073	1.54184
Crystal system	monoclinic	triclinic	triclinic	monoclinic
Space group	<i>P</i> ₂ / <i>c</i>	<i>P</i> -1	<i>P</i> -1	<i>P</i> ₂ / <i>n</i>
<i>a</i> (Å)	10.6451(3)	9.3341(5)	9.1122(5)	10.4279(2)
<i>b</i> (Å)	9.0121(2)	13.3350(7)	12.2204(6)	26.2013(5)
<i>c</i> (Å)	34.8130(9)	13.8294(7)	15.2059(8)	14.7691(3)
α (°)	90	96.956(2)	86.058(2)	90
β (°)	92.792(2)	93.676 (2)	81.427(2)	91.712(2)
γ (°)	90	102.477(2)	83.050(2)	90
<i>V</i> (Å ³)	3335.81(15)	1661.07(15)	1659.81(15)	4033.48(14)
<i>Z</i>	4	2	1	4
<i>D</i> _{calc} (g·cm ⁻³)	1.415	1.425	1.419	1.506
μ (mm ⁻¹)	4.849	1.021	1.019	6.530
<i>F</i> (000)	1472.0	736.0	733.0	1872.0
Crystal size (mm ³)	0.18 × 0.17 × 0.16	0.18 × 0.16 × 0.15	0.19 × 0.18 × 0.17	0.18 × 0.15 × 0.14
2 θ range (°)	8.316–132.006	6.046–50.018	5.954–50.016	9.024–132.016
Index ranges	–12 ≤ <i>h</i> ≤ 12, –6 ≤ <i>k</i> ≤ 10, –29 ≤ <i>l</i> ≤ 41	–11 ≤ <i>h</i> ≤ 11, –15 ≤ <i>k</i> ≤ 15, –16 ≤ <i>l</i> ≤ 16	–10 ≤ <i>h</i> ≤ 10, –14 ≤ <i>k</i> ≤ 14, –18 ≤ <i>l</i> ≤ 18	–12 ≤ <i>h</i> ≤ 11, –31 ≤ <i>k</i> ≤ 21, –17 ≤ <i>l</i> ≤ 17
Reflections collected/unique	9608/5797 <i>R</i> _{int} = 0.0523, <i>R</i> _{sigma} = 0.0609	30,051/5842 <i>R</i> _{int} = 0.0258, <i>R</i> _{sigma} = 0.0191	30,083/5833 <i>R</i> _{int} = 0.0284, <i>R</i> _{sigma} = 0.0229	13,326/6995 <i>R</i> _{int} = 0.0468, <i>R</i> _{sigma} = 0.0556
Data/restraints/parameters	5797/0/371	5842/1/371	5833/48/409	6995/24/470
Completeness (%)	99.3	99.7	99.8	99.4
Goodness of fit on <i>F</i> ²	1.184	1.085	1.035	1.037
Final <i>R</i> indices (<i>I</i> > 2 σ [<i>I</i>])	<i>R</i> ₁ = 0.0828, <i>wR</i> ₂ = 0.2098	<i>R</i> ₁ = 0.0272, <i>wR</i> ₂ = 0.0683	<i>R</i> ₁ = 0.0305, <i>wR</i> ₂ = 0.0739	<i>R</i> ₁ = 0.0583, <i>wR</i> ₂ = 0.1545
<i>R</i> indices (all data)	<i>R</i> ₁ = 0.0924, <i>wR</i> ₂ = 0.2149	<i>R</i> ₁ = 0.0315, <i>wR</i> ₂ = 0.0706	<i>R</i> ₁ = 0.0384, <i>wR</i> ₂ = 0.0784	<i>R</i> ₁ = 0.0663, <i>wR</i> ₂ = 0.1646
Largest diff peak and hole (e ⁻ ·Å ⁻³)	1.06/–0.51	0.37/–0.41	0.36/–0.32	1.30/–0.97

acetonitrile solvent in the reaction. The coordinates of optimized geometries are available in the Supporting Information.

3 | RESULTS AND DISCUSSION

3.1 | General features

Previous published procedure showed the reaction between RN (PPh₂)₂NiCl₂ and in situ formed Na₂dmit from CH₃ONa and (PhCO)₂dmit in absolute methanol and under nitrogen atmosphere^[46] only produced low yields of dmit nickel complexes. This study adopted a modified procedure by Jeon et al.^[49]; the complexes [RN (PPh₂)₂Ni(dmit)] (**1–4**) were prepared from RN (PPh₂)₂NiCl₂ and (*n*-Bu)₂Sn(dmit) in CH₂Cl₂ and acetone solutions at room temperature with 73–86% yields, as shown in Scheme 1. Results show that this modified synthetic route for **1–4** is simple and efficient, because this reaction route does not require anhydrous and oxygen-free reaction conditions; **1–4** are air-stable green solids and soluble in CH₂Cl₂, CHCl₃, MeCN, and DMF.

3.2 | Spectroscopic characterizations

The structures of **1–4** have been fully characterized by the elemental analysis, FTIR, UV-vis, ¹H, ¹³C{¹H}, and ³¹P{¹H} NMR spectroscopies. Their FTIR and NMR spectra are shown in Figures S1–S16.

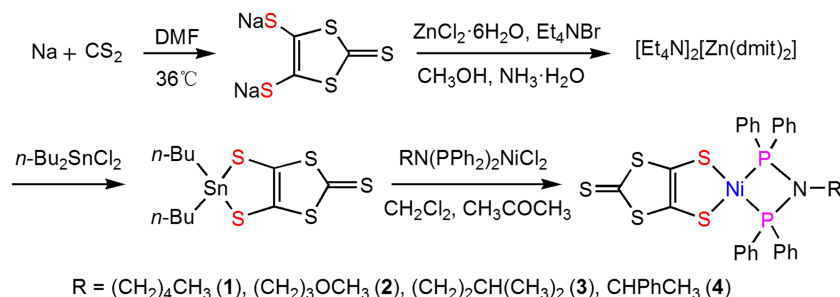
The FTIR spectra of **1–4** all display a strong absorption band in the range of 828–889 cm⁻¹ for the P–N–P bending vibration in the RN (PPh₂)₂ ligands^[37] and one strong absorption band at about 1051 cm⁻¹ for the C=S stretching vibration of the dmit ligands.^[71,72] The strong absorption bands in the range of 1097–1105 cm⁻¹ are assigned to the C–S stretching vibrations of the dmit ligands.^[72]

The ¹H NMR spectra of **1–3** display one double doublet at 7.83 ppm, two triplets at 7.52 and 7.62 ppm assigned to the phenyl protons of the PPh₂ moieties.

While the phenyl proton signals of the PPh₂ groups for **4** exhibit one multiplet (7.52–7.64 ppm), one double triplet (7.47 ppm), and two double doublets (7.82 and 7.91 ppm). Such discrepancies are most likely due to the presence of chiral α-carbon atom connected to nitrogen atom of the *N*-1-phenylethyl bis (diphenylphosphanyl) amine ligand.^[40] The ¹H NMR spectrum of **4** demonstrates one doublet at 6.62 ppm and two triplets at 6.93 and 7.08 ppm for the phenyl protons of the CH₃CHPh moiety. The proton signals of the CH₂N fragment appear one triplet at 2.92 ppm with the coupling constant of *J* = 5.7 Hz for **2**, one multiplet in 2.85–2.96 for **1**, and one multiplet in 2.83–2.99 ppm for **3**, respectively, while the CHN proton signal for **4** also presents one multiplet signal in the region of 4.47–4.58 ppm.

For the ¹³C{¹H} NMR spectra, the phenyl carbons of the PPh₂ moieties for **1–3** display one singlet around 129.28 ppm and three triplets at about 129.57, 133.10, and 138.80 ppm, respectively. The phenyl carbons of the PPh₂ moiety for **4** show four triplets at 129.32, 133.27, 133.71, and 138.81 ppm. For **1–3**, one singlet in the range of 129.26–129.78 ppm and one singlet around 221.50 ppm are assigned to the S₂C=CS₂ and S=C groups of the dmit ligand, respectively, while the S₂C=CS₂ and S=C carbon signals for **4** appear two singlets (132.87 and 133.00 ppm) and one singlet (221.42 ppm). In addition, **4** shows additional three singlets at 128.17, 128.77, and 128.98 ppm and one triplet at 139.26 ppm, which could be assigned to the phenyl carbons in the CH₃CHPh unit. Moreover, the carbon signals for NCH₂ groups of **1–3** display one triplet in the range of 46.19–48.86 ppm, while the CHN group of **4** appears one triplet at 62.09 ppm.

Correspondingly, the ³¹P{¹H} NMR spectra of **1–4** demonstrate only one singlet at 59.28, 58.56, 58.40, and 62.10 ppm, respectively. These chemical shifts are consistent with those of the analogous nickel complexes (57.47–67.16 ppm) such as [PhCH₂N(PPh₂)₂Ni(edt)], [CH₃(CH₂)₃N(PPh₂)₂Ni(pdt)], and [CH₃S(CH₂)₃N(PPh₂)₂Ni(bdt)].^[40,60,61] This can be assigned to the two phosphorus atoms of the RN (PPh₂)₂ ligand coordinated to nickel atom, which has been verified by X-ray crystallography in the following section.



SCHEME 1 Synthetic scheme of **1–4**

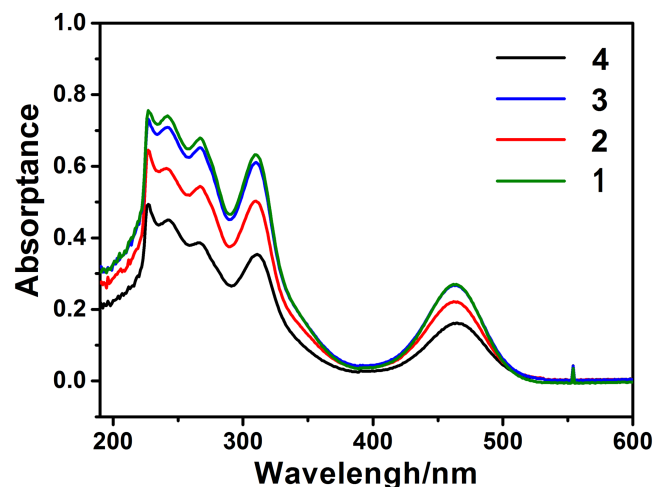


FIGURE 1 Ultraviolet-visible (UV-vis) absorption spectra of **1–4** in MeCN at room temperature

The UV-vis spectra of **1–4** were collected in MeCN at room temperature and are presented in Figure 1. Their UV-vis spectra are almost identical and show five absorption bands around 227, 241, 266, 310, and 463 nm, respectively. The low intensity band at 463 nm is assigned to the metal to ligand charge transfer (MLCT) transition from nickel to phosphorus and nickel to sulfur.^[73,74] The rest four absorption bands may be assigned as intraligand charge transfer (ILCT) $\pi \rightarrow \pi^*$ transitions of both R_2N (PPh_2)₂ and dmit ligand.^[33,59,72–74]

3.3 | Crystal structures

The molecular structures of **1–3** and **4·2CH₂Cl₂** are shown in Figures 2–5. The selected bond lengths and angles are listed in Table 2. The C26–C29 atoms of

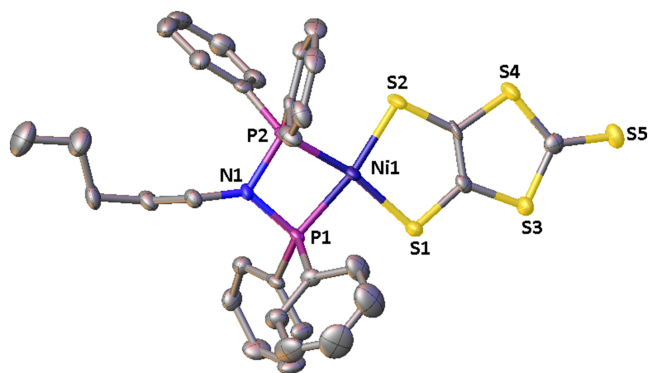


FIGURE 2 Molecular structure of **1** with displacement ellipsoids at the 50% probability level. Hydrogen atoms have been omitted for clarity

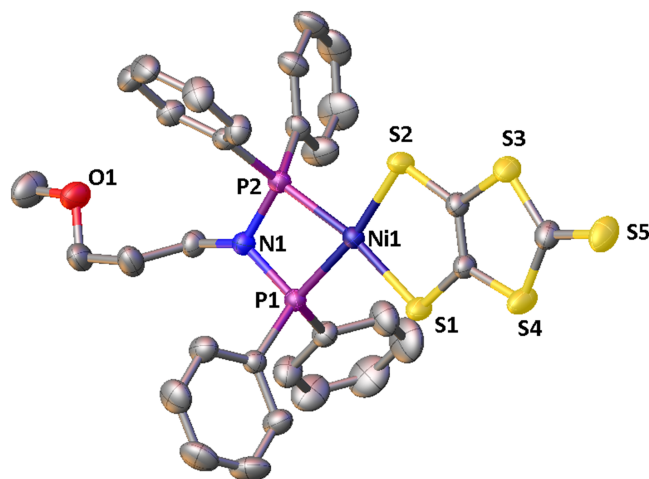


FIGURE 3 Molecular structure of **2** with displacement ellipsoids at the 50% probability level. Hydrogen atoms have been omitted for clarity

isopentyl group for **3** and one CH_2Cl_2 solvent molecular for **4·2CH₂Cl₂** are in disordered states.

As shown in Figures 2–5, all complexes contain one mononuclear nickel atom ligated by two phosphorus atoms of RN (PPh_2)₂ and two sulfur atoms of dmit ligands. Their structures are all isostructural in which the nickel atom adopts a slightly distorted square-planar coordination, which deviations from the mean plane formed by P1, P2, S1, and S2 atoms. The sum of the angles around the nickel atom is 359.99° (for **1**), 360.06° (for **2**), 360.35° (for **3**), and 360.33° (for **4·2CH₂Cl₂**), respectively. The Ni–S and Ni–P bond lengths for **1–3** and **4·2CH₂Cl₂** are comparable with those determined for $[RN$ (PPh_2)₂Ni(bdt)] ($R = (CH_2)_3OCH_3$, $(CH_2)_3SCH_3$, and $CHPhCH_3$ [Ni–S: 2.1430–2.1567 Å; Ni–P: 2.1348–2.1701 Å]),^[40] (dppv)Ni (dmit) (Ni–S: 2.1601 [6] and 2.1693[6] Å; Ni–P: 2.1507[6], and 2.1520

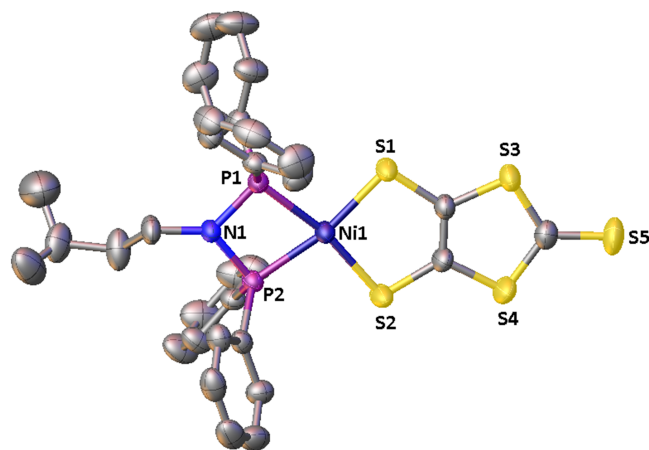


FIGURE 4 Molecular structure of **3** with displacement ellipsoids at the 50% probability level. Hydrogen atoms have been omitted for clarity

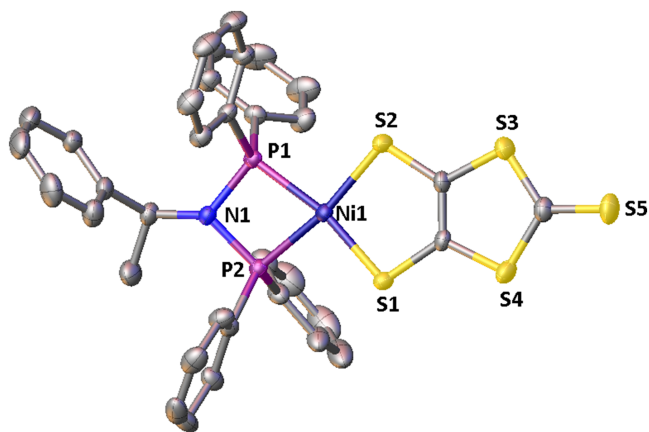


FIGURE 5 Molecular structure of **4**·2CH₂Cl₂ with displacement ellipsoids at the 50% probability level. Hydrogen atoms and CH₂Cl₂ molecules have been omitted for clarity

[7] Å),^[46] (dppv)Ni(dmio) (Ni–S: 2.1681[7] and 2.1642 [7] Å; Ni–P: 2.1570[7] and 2.1606[9] Å),^[46] and [*i*-BuN(PPh₂)₂Ni(edt(CH₃)₂)] (Ni–S: 2.1663[9] and 2.1681 [8] Å; Ni–P: 2.1506[9] and 2.1561[9] Å).^[75] The measured P1–Ni1–P2 and S1–Ni1–S2 bond angles for **1–3** and **4**·2CH₂Cl₂ are close to those of the analogous nickel complexes.^[32,36,40,46,59,61,75] The dmit ligands for the complexes are all coplanar configuration due to the fully conjugated π bonds feature, whereas the four-membered metallocycle Ni1P1N1P1A are almost coplanar with the mean deviations of 0.046 for **1**, 0.018 for **2**, 0.005 for **3**, and 0.068° for **4**·2CH₂Cl₂, respectively. This suggests that the N1 atom in RN(PPh₂)₂ ligand adopts sp^2 hybridization due to the influence of coordination.^[32]

3.4 | Thermogravimetric analyses

The thermogravimetric measurements for **1–4** were recorded on a NETZSCH STA 409 PC/PG instrument with a flow of 100 mL min⁻¹ nitrogen atmosphere at a heating rate of 10.0°C min⁻¹ in the range of 25–700°C. As illustrated in Figure 6, only **1** exhibits a slight weightlessness under 100°C, which may be caused by the evaporation of bound water; **1**, **3**, and **4** show two-step decompositions that occur in the temperature ranges of 288.3–319.6 and 346.1–390.4°C by weight loss of 31.01 and 32.22 (for **1**), 33.59 and 25.46 (for **3**), and 17.36 and 39.00% (for **4**), respectively. Whereas **2** presents only one-step decomposition by weight loss of 59.79% in the range of 314.8–410.9°C. According to the TGA analysis, the order of thermal stability of the four complexes can be summarized as follows: **4** > **3** > **2** > **1**.

3.5 | Electrochemical studies

The electrochemical properties of **1–4** were measured by CV in MeCN with 0.1 M *n*-Bu₄NPF₆ as the supporting electrolyte under nitrogen atmosphere. The electrochemical data are presented in Table 3. The CV for **1** displays two sets of redox peaks within the potential windows, as presented in Figure 7. A reversible reduction peak at $E_{pc} = -1.60$ V versus Fc⁺/Fc for **1** can be ascribed to one-electron reduction of Ni^{II} to Ni^I.^[32,35,76,77] The irreversible oxidation peak at $E_{pa} = 0.22$ V versus Fc⁺/Fc can be assigned to the oxidation of *N*-butyl bis(diphenylphosphanyl)amine ligand.^[78] Similarly, **2–4** also show one reversible reduction peak for Ni^{II}/Ni^I couple at $E_{pc} = -1.58$, -1.58 , and -1.66 V versus Fc⁺/Fc and the irreversible oxidation event at $E_{pa} = 0.22$ – 0.24 V versus Fc⁺/Fc for bis(diphenyl-phosphanyl)amine ligands, respectively (see Figures S21, S27, and S33).

Variable-scan rate studies of **1–4** demonstrate linear relationships of the currents to the square root of the scan rate ($\nu^{1/2}$) for the Ni^{II}/Ni^I events, indicating diffusion-controlled processes (Figures 8, S22, S28, and S34),^[34,40,57] where the electrochemical active species are freely diffusing in the solution and the calculated diffusion coefficients are determined to be 1.47×10^{-5} , 1.47×10^{-5} , 1.20×10^{-5} , and 2.24×10^{-5} cm²·s⁻¹, respectively.^[77,79]

3.6 | Electrocatalytic hydrogen evolution

To determine the electrocatalytic activities of complexes **1–4**, the CVs of **1–4** in MeCN have been explored with the addition of TFA ($pK_a^{MeCN} = 12.7$, $E^\circ = 0.89$ V vs. Fc⁺/Fc.^[77]). As shown in Figure 9, the successive addition of TFA to **1** in MeCN, CV curves display a significant increased cathodic current near $E_{pc} = -1.60$ V versus Fc⁺/Fc concomitant with the formation of gas bubbles, which is confirmed to be H₂ by gas chromatography (GC)-TCD analysis (see Figure S40). Meanwhile, the maximum peak gradually shifts to more negative potentials. These phenomena indicate that **1** can effectively catalyze protons reduction to hydrogen in the presence of TFA in the electrochemical condition.^[34,40,77]

A number of control experiments were also carried out to confirm that **1** is responsible for the catalysis. For example, the current peak of hydrogen evolution of $E_{pc} = -2.07$ V versus Fc⁺/Fc by glassy carbon working electrode is observed with 10-mM TFA (Figure S19). However, the reduction peak current for **1** is observed at $E_{pc} = -1.63$ V versus Fc⁺/Fc in the presence of 10-mM TFA. The shift of reduction peak current of **1** suggests that the electrocatalytic activity is entirely from complex

TABLE 2 Selected bond lengths (Å) and bond angles (°) for **1–3** and **4·2CH₂Cl₂**

1			
Ni1–S1	2.152(2)	Ni1–P1	2.146(2)
Ni1–S2	2.163(2)	Ni1–P2	2.130(2)
P1–N1	1.696(5)	P2–N1	1.707(6)
S5–C32	1.644(8)	P1–Ni1–P2	73.53(7)
P1–Ni1–S1	93.93(8)	S1–Ni1–S2	95.44(8)
P2–Ni1–S2	97.16(8)	N1–P1–Ni1	94.1(2)
P1–N1–P2	97.5(3)	N1–P2–Ni1	94.3(2)
C30–S1–Ni1	100.3(2)	C30–S3–C32	97.9(3)
C31–S2–Ni1	99.7(2)	S3–C32–S4	111.8(4)
C31–S4–C32	98.6(4)	S2–C31–S4	122.3(4)
S5–C32–S3	123.4(4)		
2			
Ni1–S1	2.1664(5)	Ni1–P1	2.1506(5)
Ni1–S2	2.1618(5)	Ni1–P2	2.1566(5)
P1–N1	1.6928(15)	P2–N1	1.6938(15)
S5–C31	1.655(2)	P1–Ni1–P2	73.682(19)
P1–Ni1–S1	94.94(2)	S1–Ni1–S2	94.83(2)
P2–Ni1–S2	96.54(2)	N1–P1–Ni1	93.54(5)
C30–S1–Ni1	100.22(7)	N1–P2–Ni1	93.30(5)
C29–S2–Ni1	100.32(6)	P1–N1–P2	99.39(8)
C30–S4–C31	97.97(10)	C29–S3–C31	97.92(9)
S5–C31–S3	123.44(13)	S3–C31–S4	112.45(11)
S3–C31–S4	112.45(11)		
3			
Ni1–S1	2.1564(6)	Ni1–P1	2.1479(6)
Ni1–S2	2.1556(7)	Ni1–P2	2.1493(6)
P1–N1	1.6947(18)	P2–N1	1.6942(18)
S5–C32	1.654(2)	P1–Ni1–P2	73.75(2)
P1–Ni1–S1	96.05(2)	S1–Ni1–S2	94.84(2)
P2–Ni1–S2	95.71(2)	N1–P2–Ni1	93.55(6)
C30–S1–Ni1	100.63(8)	N1–P1–Ni1	93.59(6)
C31–S2–Ni1	100.59(8)	P1–N1–P2	99.10(9)
C31–S4–C32	98.14(12)	C30–S3–C32	97.97(11)
S5–C32–S3	123.99(16)	S2–C31–S4	122.25(14)
S3–C32–S4	112.26(14)		
4·2CH₂Cl₂			
Ni1–S1	2.1669(10)	Ni1–P1	2.1417(10)
Ni1–S2	2.1622(11)	Ni1–P2	2.1311(10)
P1–N1	1.710(3)	P2–N1	1.703(3)
S5–C35	1.652(4)	P1–Ni1–P2	73.17(4)
P1–Ni1–S2	95.97(4)	S1–Ni1–S2	95.29(4)
P2–Ni1–S1	95.90(4)	N1–P2–Ni1	94.83(11)
C33–S1–Ni1	100.05(13)	N1–P1–Ni1	94.24(10)

(Continues)

TABLE 2 (Continued)

1			
C34-S2-Ni1	100.25(13)	P1-N1-P2	96.51(15)
C33-S4-C35	97.99(19)	C34-S3-C35	97.94(19)
S5-C35-S3	123.9(3)	S1-C33-S4	122.1(2)
S3-C35-S4	112.6(2)		

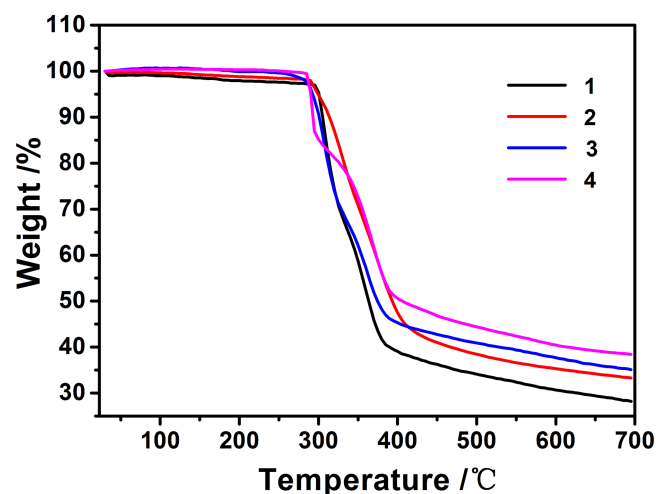


FIGURE 6 Thermogravimetric analysis curves for 1-4

catalyst **1**. Noticeably, the oxidation peak current is not affected much under the acidic and electrochemical conditions, as shown in Figure 9.

Similarly, **2-4** also show similar electrocatalytic behaviors to that of **1** for the reduction of protons in the presence of TFA in MeCN (Figures S23, S29, and S35). In addition, the catalytic currents (i_{cat}) for **1-4** with the addition of 10-mM TFA show linear dependences on the square root of the scan rate ($\nu^{1/2}$) (Figures 10, S24, S30, and S36), respectively, suggesting that their electrocatalysis is diffusion-controlled processes.^[34,40,57] And the corresponding diffusion coefficients for **1-4** in the presence of 10-mM TFA are

3.22×10^{-3} , 3.83×10^{-3} , 3.65×10^{-3} , and $3.63 \times 10^{-3} \text{ cm}^2 \cdot \text{s}^{-1}$, respectively. Moreover, the standard rinse experiments for **1-4** also indicate that the electrocatalysis is only initiated by molecular species in solution and not by the unknown nanoparticle materials on the electrode surface (Figures S20, S26, S32, and S38).^[33,34] These findings suggest that **1-4** all have efficient reactivity as homogeneous molecular catalysts for reduction protons, and the as-observed catalytic waves correspond to hydrogen evolution.^[34,56,57]

Furthermore, the $i_{\text{cat}}/i_{\text{pc}}$ ratio of the Ni^{II}/Ni^I couple can be used as an indicator for the catalytic efficiency of different catalytic complexes, where the i_{pc} and i_{cat} are the peak currents observed for the complex catalysts in the absence of and in the presence of TFA. A higher value of $i_{\text{cat}}/i_{\text{pc}}$ suggests a faster catalysis reaction.^[37,80] As showed in Table 3, $i_{\text{cat}}/i_{\text{pc}}$ values of **1-4** with the addition of 120-mM TFA exhibit the catalytic efficiency order of **2** > **3** > **1** > **4**. This result shows that **2** as molecular electrocatalyst has a higher catalytic efficiency than other complexes. Interestingly, the plots of $i_{\text{cat}}/i_{\text{pc}}$ for **1-4** versus the square root of the amount of the TFA added demonstrate linear correlations, indicating first-order dependence of the catalytic rate on TFA concentration (Figures 9, S23, S29, and S35).^[24,34] Also, the catalytic currents reveal linear dependency on the concentrations of **1-4** (Figures 11, S25, S31, and S37), which suggests first-order catalytic reaction.

The TOF and the overpotential (η) of the catalytic reaction can be used to quantitatively evaluate the

Complex	E_{pc} (V)	E_{pa} (V)	i_{pc} (μA) ^[a]	i_{cat} (μA) ^[b]	$i_{\text{cat}}/i_{\text{pc}}$
1	-1.60	+0.22	10.23	1545.43	151.07
2	-1.58	+0.24	11.01	1812.56	164.63
3	-1.58	+0.24	10.11	1564.34	154.73
4	-1.66	+0.22	12.74	1554.18	121.99

TABLE 3 The electrochemical data of **1-4** (vs. Fc⁺/Fc) in MeCN

^aThe i_{pc} is the cathodic peak current at Ni^{II}/Ni^I event observed for 0.5-mM catalyst in the absence of TFA in MeCN (0.1 M *n*-Bu₄NPF₆, glassy carbon electrode, potential vs. Fc⁺/Fc, 100 mV·s⁻¹ scan rate).

^bThe i_{cat} is the catalytic cathodic peak current for 0.5-mM catalyst observed in the presence of 120-mM TFA in MeCN (0.1 M *n*-Bu₄NPF₆, glassy carbon electrode, potential vs. Fc⁺/Fc, 100 mV·s⁻¹ scan rate).

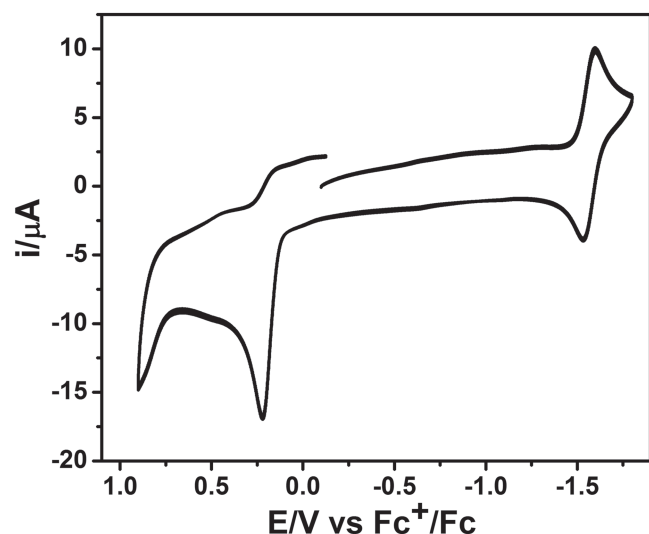


FIGURE 7 Cyclic voltammogram of 0.5-mM **1** in MeCN (0.1 M *n*-Bu₄NPF₆, glassy carbon electrode, potential vs. Fc⁺/Fc, 100 mV s⁻¹ scan rate)

catalytic activities.^[77,79] The detail calculation of TOF and the overpotential (η) are presented in the Supporting Information, and the results are summarized in Table 4. The TOF values of the complex-catalyzed TFA reduction can be calculated from CVs by comparing the ratio of $i_{\text{cat}}/i_{\text{pc}}$ (see the Supporting Information), which are 4336 (for **1**), 5149 (for **2**), 4548 (for **3**), and 2827 s⁻¹ (for **4**), when 120-mM TFA is added. Following the method of Fourmond and coworkers,^[81] the overpotential (η) required to attain half of the overall catalytic current determined for **1–4** evaluate 0.79, 0.72, 0.76, and 0.78 V, respectively (see the Supporting Information). Under the

identical conditions, the TOF values of **1–4** for hydrogen production are 8–14 times than those of analogous nickel complexes [RN (PPh₂)₂Ni(mnt)], and the corresponding overpotentials are slightly greater than those of [RN (PPh₂)₂Ni(mnt)].^[78] The difference in catalytic activity for hydrogen evolution is mainly caused by the significant electronic difference between the dithiolene ligands, namely, that dmit ligand is an electronic donor while mnt ligand is an acceptor. The secondary reason may come from the slightly difference for electrocatalytic hydrogen production mechanism, which is described below.

3.7 | Evaluation of stability for the electrocatalytic complexes

The stability of **1–4** was evaluated and monitored with the UV–vis absorption spectra in the presence of concentrate TFA in MeCN and under the electrocatalytic conditions. The MeCN solutions of **1–4** are insensitive to air as indicated by temporal evolution of their UV–vis absorption spectra (Figure S17). And as depicted in Figure S18, the UV–vis absorption spectra of **1–4** in MeCN with 50-mM TFA were unchanged for 12 h, indicating **1–4** all have good acid tolerance. Furthermore, the bulk electrolysis experiments of **1–4** in MeCN in the presence of 50-mM TFA at -1.6 V versus Fc⁺/Fc showed little change of the UV–vis absorption spectra for 1.5 h, compared with before electrolysis, and the color of the solution remained unchanged, and no precipitation was also observed (Figure S39). The spectroelectrochemical experiments suggest that the catalysts for hydrogen production are

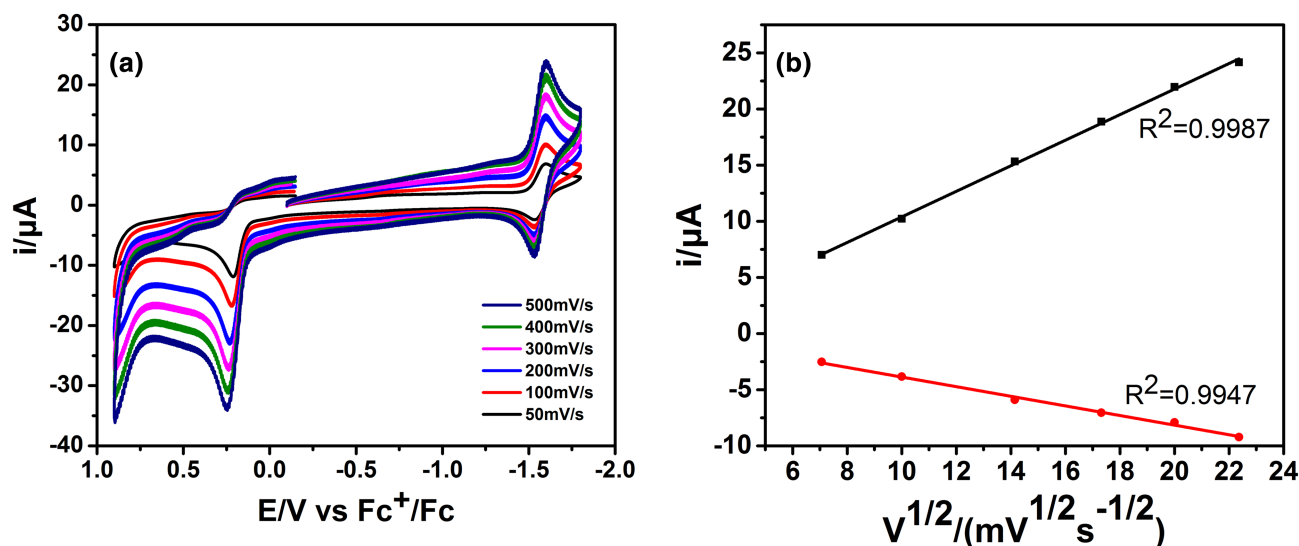


FIGURE 8 (a) Cyclic voltammograms of 0.5-mM **1** in MeCN at different scan rate (0.1-M *n*-Bu₄NPF₆, glassy carbon electrode, potential vs. Fc⁺/Fc). (b) Plots of i_{pc} and i_{pa} for the Ni^{II}/Ni^I couple versus $v^{1/2}$ for 0.5-mM **1** in MeCN

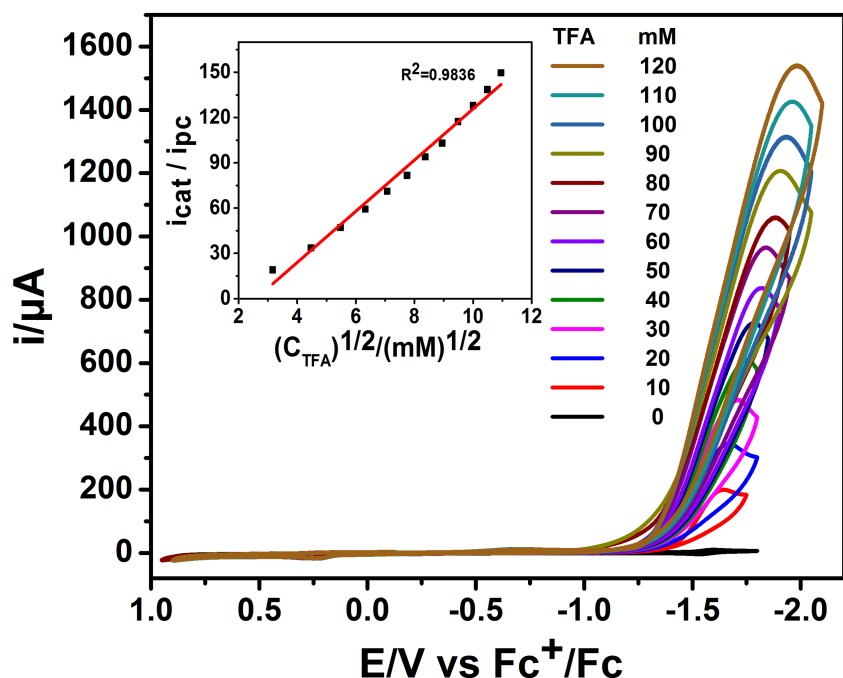


FIGURE 9 Cyclic voltammograms of 0.5-mM **1** in the presence of 0- to 120-mM TFA in MeCN (0.1-M $n\text{-Bu}_4\text{NPF}_6$, glassy carbon electrode, potential vs. Fc^+/Fc , $100\text{ mV}\cdot\text{s}^{-1}$ scan rate). Inset: Plots of the plateau current ($i_{\text{cat}}/i_{\text{pc}}$) of 0.5-mM **1** against the square root of TFA concentration

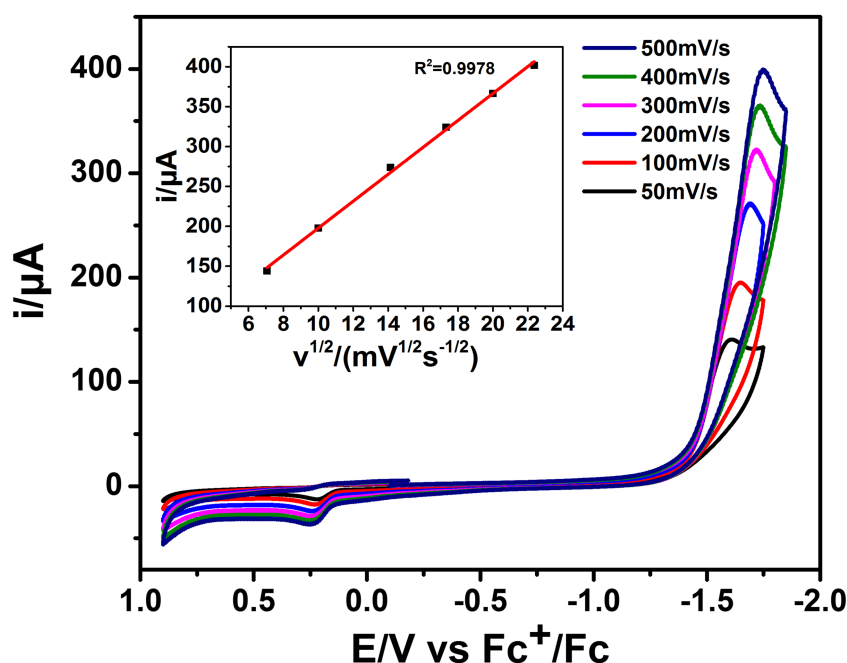


FIGURE 10 Cyclic voltammograms of 0.5-mM **1** at different scan rate in the presence of 10-mM TFA in MeCN (0.1-M $n\text{-Bu}_4\text{NPF}_6$, glassy carbon electrode, potential vs. Fc^+/Fc). Inset: Plots of i_{pc} versus $v^{1/2}$ for 0.5-mM **1** in MeCN in the presence of 10-mM TFA

likely relatively stable even under the acidic and electrochemical conditions.^[18,24,33,34] In contrast, the electrocatalytic hydrogen evolution complex $[\text{CpCo}(\text{N}^{\wedge}\text{N})(\text{MeCN})(\text{ClO}_4)_2]$ is unstable when using DMFH^+/DMF buffer as the proton source under the electrocatalytic conditions.^[19] Similarly, a high-efficient hydrogen evolution electrocatalyst $[(\text{dppp})\text{Ni}(\text{pdt})]$ is also unstable and degrades to an electrode-adsorbed film under the electrochemical conditions.^[35] Therefore, with the combination of the standard rinse experiments (Figures S20, S26, S32, and S38), all these results support that **1–4** are low-cost

and robust molecular electrocatalysts for hydrogen evolution using TFA as the proton source.

3.8 | Catalytic mechanistic studies for hydrogen evolution

Molecular catalysis of hydrogen evolution through the electrochemical protons reduction can proceed through homolytic route or heterolytic route.^[82] Based on the abovementioned electrochemical observations and the

FIGURE 11 Cyclic voltammograms of **1** (0.1, 0.2, 0.3, 0.4, and 0.5 mM) in the presence of 10-mM TFA in MeCN (0.1-M *n*-Bu₄NPF₆, glassy carbon electrode, potential versus Fc⁺/Fc, 100 mV·s⁻¹ scan rate). Inset: Plots of *i*_{cat} versus catalyst concentration (0.1, 0.2, 0.3, 0.4, and 0.5 mM) for **1** in MeCN in the presence of 10-mM TFA

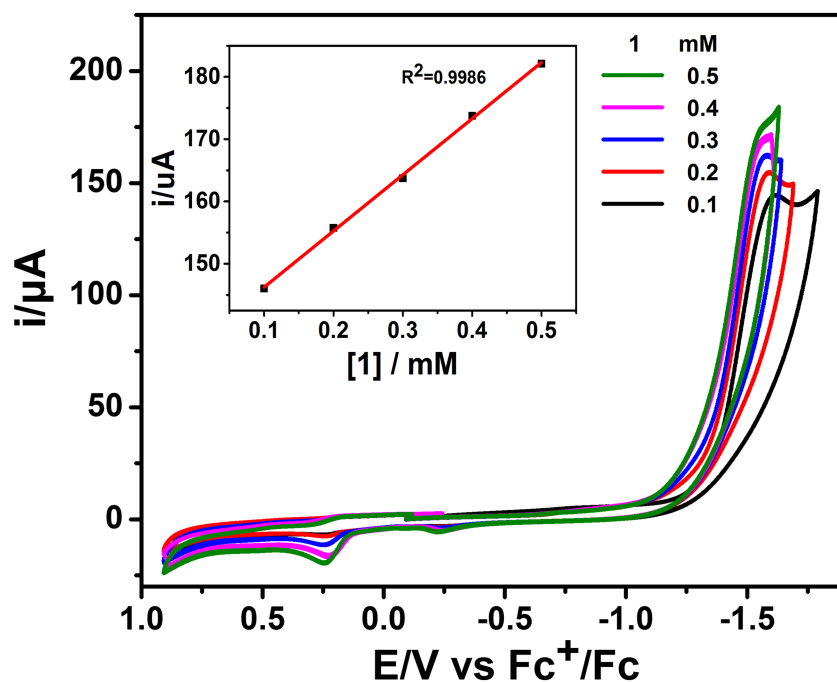


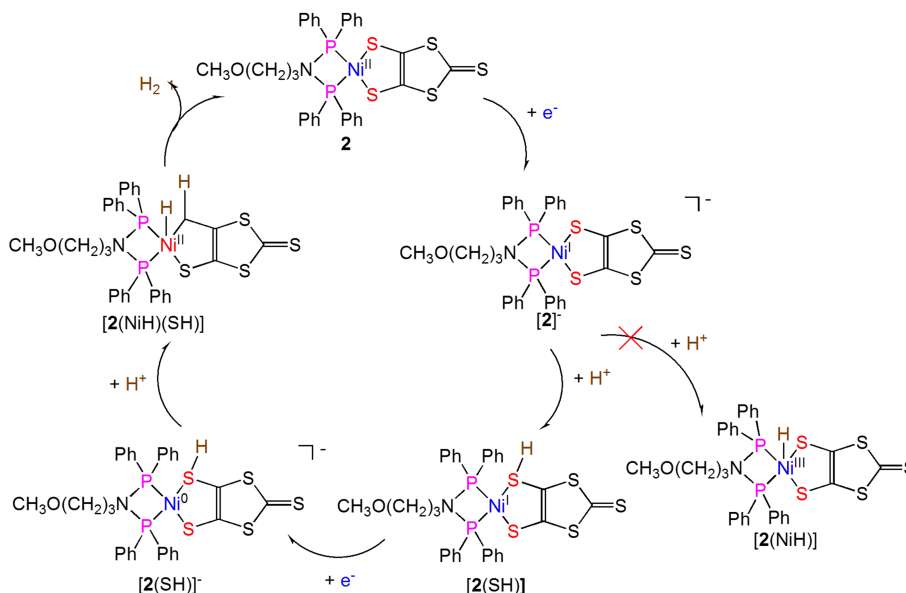
TABLE 4 The values of the turnover frequency (TOF), overpotential (η), and diffusion coefficient (D_0 and D_1) for **1–4**^[a]

Complex	TOF (s ⁻¹)	η (V)	D_0 (cm ² ·s ⁻¹) ^[b]	D_1 (cm ² ·s ⁻¹) ^b
1	4336	0.79	1.47×10^{-5}	3.22×10^{-3}
2	5149	0.72	1.47×10^{-5}	3.83×10^{-3}
3	4548	0.76	1.20×10^{-5}	3.65×10^{-3}
4	2827	0.78	2.24×10^{-5}	3.63×10^{-3}

^aThe data of the turnover frequency (TOF) and overpotential (η) were calculated by the methods of Supporting Information.

^bThe diffusion coefficients of D_0 (without TFA) and D_1 (with 10-mM TFA) were determined using the Randles–Sevcik equation (see Supporting Information).

SCHEME 2 The possible catalytic mechanism for protons reduction by **2**



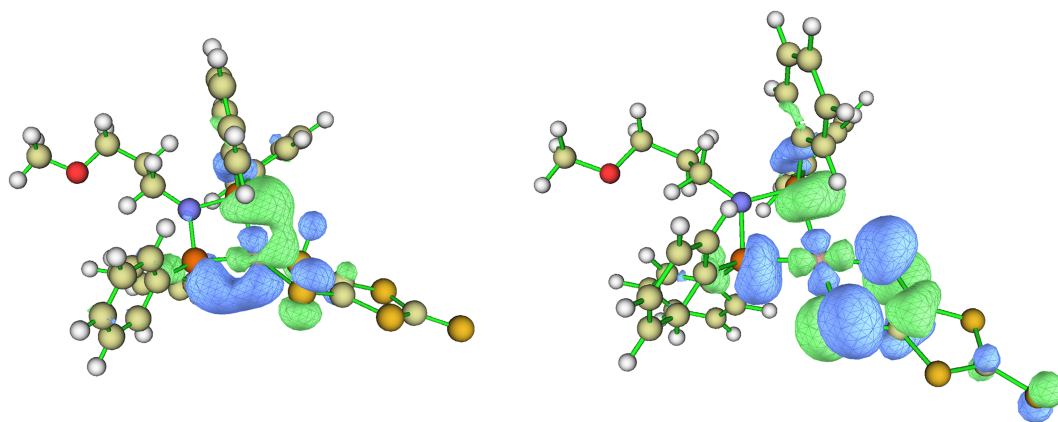


FIGURE 12 Single electron occupied highest occupied molecular orbital (HOMO) of $[2]^-$ (left) and HOMO of $[2(\text{SH})]^-$ (right) for catalyst **2** by using B3LYP/6-311G(d, p)

previously studies,^[34,56] a heterolytic ECEC mechanism is proposed for hydrogen production of **1–4** in the presence of TFA. The following experimental results support the ECEC mechanism: (a) The catalytic peak current is proportion to the square root of the TFA concentration; (b) the UV-vis absorption spectra for **1–4** are not affected by the presence of TFA; (c) the catalytic peak is observed at a potential close to the $\text{Ni}^{\text{II}}/\text{Ni}^{\text{I}}$ reduction potential.

DFT calculations are also employed to investigate the possible reaction pathways for hydrogen evolution by catalysts. Scheme 2 illustrates the reaction pathway of the proposed ECEC mechanism with catalyst **2** as a model. Firstly, one-electron reduction of neutral complex **2** forms a monoanionic species $[2]^-$ at -1.63 V versus Fc^+/Fc . Secondly, the protonation of $[2]^-$ at sulfur or nickel atoms by TFA could yield either $[2(\text{NiH})]$ or $[2(\text{SH})]$ (where S represent the dmit ligand), respectively. The calculation results indicate that the most favorable protonation site of $[2]^-$ is on one of the chelating sulfur atoms of the dmit ligand. The nickel-protonated species $[2(\text{NiH})]$ is less stable by $36 \text{ kJ}\cdot\text{mol}^{-1}$ than sulfur-protonated species $[2(\text{SH})]$. In this single electron occupied highest occupied molecular orbital (HOMO) of $[2]^-$, indeed, S1 and S2 atoms contribute 37%, Ni atom contributes 23%, and P1 and P2 atoms contribute 19%, respectively (Figure 12). This result suggests that the chelating sulfur atoms serve as the proton relays. The sulfur protonation of **2** is similar to the homoleptic complex $[\text{n-Bu}_4\text{N}][\text{Ni}(\text{mnt})_2]$ but in contrast to the heteroleptic complexes $[\text{RN}(\text{PPh}_2)_2\text{Ni}(\text{mnt})]$. For example, DFT study of $[\text{n-Bu}_4\text{N}][\text{Ni}(\text{mnt})_2]$ by Zarkadoulas and coworker showed that the protonation occurs on the sulfur atom of the dianion $[\text{Ni}(\text{mnt})_2]^{2-}$ ^[57]; while the study on $[\text{RN}(\text{PPh}_2)_2\text{Ni}(\text{mnt})]$ by Mou et al. revealed that the neutral nickel species is reduced to the monoanion, followed by the protonation on the nickel atom.^[78] Thirdly, a

second electron reduction of $[2(\text{SH})]$ affords monoanionic species $[2(\text{SH})]^-$. However, the subsequent second protonation of $[2(\text{SH})]^-$ leads only to protonate on the nickel ion, namely, $[2(\text{NiH})(\text{SH})]$. The HOMO orbital analysis of $[2(\text{SH})]^-$ (Figure 12) reveals only 7% contribution of S1 and S2 atoms, 27% contribution from P1 and P2 atoms, and 52% contribution from Ni atom. This is different from $[\text{n-Bu}_4\text{N}][\text{Ni}(\text{mnt})_2]$, where the diprotonations occur on two sulfur atoms from two different mnt ligands and yields a $[\text{Ni}(\text{mntH})(\text{mntH})]^-$ species. Interestingly, this $[\text{Ni}(\text{mntH})(\text{mntH})]^-$ species is more stable than the $[(\text{NiH})(\text{mntH})(\text{mnt})]^-$ species.^[57] Close examining the second protonation species $[2(\text{NiH})(\text{SH})]$ shows that the S–H bond is *syn* to the $\text{Ni}^{\text{II}}\text{–H}$ bond, which is similar to the key intermediates $[(\text{CoH})(\text{SH})]$ of the dithiolene cobalt complexes with qpdt^{2-} , bdt^{2-} , or tdt^{2-} ligands.^[17,55] Lastly, $[2(\text{NiH})(\text{SH})]$ produces hydrogen from the hydride on the nickel ion and the proton on the sulfur atom and regenerates catalyst **2**.

4 | CONCLUSION

In summary, four new heteroleptic dmit nickel complexes with bis(diphenylphosphanyl)amine ligands, $[\text{RN}(\text{PPh}_2)_2\text{Ni}(\text{dmit})]$ (**1–4**), were synthesized with satisfactory yields by the reactions of $(\text{n-Bu})_2\text{Sn}(\text{dmit})$ and $\text{RN}(\text{PPh}_2)_2\text{NiCl}_2$ at room temperature. These four complexes were characterized by elemental analysis, spectroscopy (FTIR, UV-vis, ^1H , $^{13}\text{C}\{^1\text{H}\}$, and $^{31}\text{P}\{^1\text{H}\}$ NMR), thermogravimetric analysis, and single crystal X-ray diffraction. The crystal structures for **1–3** and **4**· $2\text{CH}_2\text{Cl}_2$ reveal that the nickel atom lies at the center but a slightly distorted square-planar geometry. In addition, the electrochemical properties of **1–4** have been measured by means of CV in MeCN. The investigation results suggest

that all complexes are robust molecular catalysts and can efficiently electrocatalyze protons reduction to hydrogen with TFA as the proton source. A possible ECEC mechanism for electrocatalytic hydrogen evolution was also examined. The DFT calculations show that the chelating sulfur atoms of the dmit ligand are preferred protonation sites than the nickel center; thus, the chelating sulfur atoms may serve as proton relays. And only the second protonation forms a [NiH(SH)] hydride intermediate. This study demonstrates that the dmit nickel complexes represent a new group of active catalysts for the reduction of protons to hydrogen.

DATA AVAILABILITY STATEMENT

The authors confirm that the data supporting the findings of this study are available within the article and its supplementary materials.

ACKNOWLEDGEMENTS

This work is supported by grants from the Open Fund Project of Sichuan Province Key Laboratory of Comprehensive Utilization of Vanadium & Titanium Resources (2018FTSZ09), the Science and Technology Bureau of Zigong City (2015HX18, 2019CXMZ01, and 2020MZGC06), the Training Program of Innovation and Entrepreneurship for Undergraduates of Sichuan University of Science and Technology (cx2019198), and the Graduate Innovation Fund Project of Sichuan University of Science and Technology (y2019023 and y2019031).

AUTHOR CONTRIBUTIONS

Tao Li: Conceptualization; investigation; visualization. **Bin Xie:** Conceptualization; funding acquisition; methodology; project administration; resources; supervision. **Jia-Xi Cao:** Investigation; methodology; visualization. **Dong-Liang Zhang:** Data curation; investigation. **Chuan Lai:** Resources; supervision. **Hua-Jun Fan:** Resources. **Bin Zhao:** Formal analysis; supervision. **Wen-Yu Mou:** Validation. **Xiao-Xue Bai:** Investigation.

CONFLICT OF INTEREST

The authors declare that they have no known competing financial interests or personal relationships that could have appeared to influence the work reported in this paper.

ORCID

Bin Xie  <https://orcid.org/0000-0002-9345-5084>

REFERENCES

- [1] M. S. Dresselhaus, I. L. Thomas, *Nature* **2001**, *414*, 332.
- [2] N. S. Lewis, *Energ. Environ. Sci.* **2016**, *9*, 2172.
- [3] K. Mgller, W. Arlt, *Energy Technol.-Ger.* **2013**, *1*, 501.
- [4] U. Eberle, M. Felderhoff, F. Schgth, *Angew. Chem. Int. Ed.* **2009**, *48*, 6608.
- [5] Z. J. Han, R. Eisenberg, *Acc. Chem. Res.* **2014**, *47*, 2537.
- [6] V. Artero, M. Fontecave, *Coord. Chem. Rev.* **2005**, *249*, 1518.
- [7] A. Zarkadoulas, M. J. Field, C. Papatriantafyllopoulou, J. Fize, V. Artero, C. A. Mitsopoulou, *Inorg. Chem.* **2016**, *55*, 432.
- [8] H. Q. Yuan, H. H. Wang, J. Kandhadi, H. Wang, S. Z. Zhan, H. Y. Liu, *Appl. Organomet. Chem.* **2017**, *31*, e3773.
- [9] M. D. Sampson, C. P. Kubiak, *Inorg. Chem.* **2015**, *54*, 6674.
- [10] E. B. Hemming, B. Chan, P. Turner, L. Corcilius, J. R. Price, M. G. Gardiner, A. F. Masters, T. Maschmeyer, *Appl. Catal. B-Environ.* **2018**, *223*, 234.
- [11] M. Y. Hu, L. Yan, J. R. Li, Y. H. Wang, P. H. Zhao, X. F. Liu, *Appl. Organomet. Chem.* **2019**, *33*, e4949.
- [12] D. Schilter, J. M. Camara, M. T. Huynh, S. Hammes-Schiffer, T. B. Rauchfuss, *Chem. Rev.* **2016**, *116*, 8693.
- [13] R. X. Li, X. T. Ren, M. Y. Tang, M. X. Chen, G. B. Huang, C. H. Fang, T. Liu, Z. H. Feng, Y. B. Yin, Y. M. Guo, S. K. Mei, J. Yan, *Appl. Catal. B-Environ.* **2018**, *224*, 772.
- [14] L. C. Song, Y. X. Wang, X. K. Xing, S. D. Ding, L. D. Zhang, X. Y. Wang, H. T. Zhang, *Chem. A Eur. J.* **2016**, *22*, 16304.
- [15] J. G. Kleingardner, B. Kandemir, K. L. Bren, *J. Am. Chem. Soc.* **2014**, *136*, 4.
- [16] L. Chen, M. Wang, K. Han, P. L. Zhang, F. Gloaguen, L. C. Sun, *Energ. Environ. Sci.* **2014**, *7*, 329.
- [17] T. Fogeron, J. P. Porcher, M. Gomez-Mingot, T. K. Todorova, L. M. Chamoreau, C. Mellot-Draznieks, Y. Li, M. Fontecave, *Dalton Trans.* **2016**, *45*, 14754.
- [18] H. L. Sun, Y. Z. Han, H. T. Lei, M. X. Chen, R. Cao, *Chem. Commun.* **2017**, *53*, 6195.
- [19] K. M. Waldie, S. K. Kim, A. J. Ingram, R. M. Waymouth, *Eur. J. Inorg. Chem.* **2017**, *2017*, 2755.
- [20] N. Queyriaux, R. T. Jane, J. Massin, V. Artero, M. Chavarot-Kerlidou, *Coord. Chem. Rev.* **2015**, *304*, 3.
- [21] T. K. Mukhopadhyay, N. L. MacLean, L. Gan, D. C. Ashley, T. L. Groy, M.-H. Baik, A. K. Jones, R. J. Trovitch, *Inorg. Chem.* **2015**, *54*, 4475.
- [22] P. L. Zhang, M. Wang, Y. Y. Yang, T. Y. Yao, L. C. Sun, *Angew. Chem. Int. Ed.* **2014**, *126*, 14023.
- [23] Z. J. Xin, S. Liu, C. B. Li, Y. J. Lei, D. X. Xue, X. W. Gao, H. Y. Wang, *Int. J. Hydrogen Energy* **2017**, *42*, 4202.
- [24] H. T. Lei, H. H. Fang, Y. Z. Han, W. Z. Lai, X. F. Fu, R. Cao, *ACS Catal.* **2015**, *5*, 5145.
- [25] H. I. Karunadasa, E. Montalvo, Y. Sun, M. Majda, J. R. Long, C. J. Chang, *Science* **2012**, *335*, 698.
- [26] V. S. Thoi, H. I. Karunadasa, Y. Surendranath, J. R. Long, C. J. Chang, *Energ. Environ. Sci.* **2012**, *5*, 7762.
- [27] H. I. Karunadasa, C. J. Chang, J. R. Long, *Nature* **2010**, *464*, 1329.
- [28] J. W. Wang, W. J. Liu, D. C. Zhong, T. B. Lu, *Coord. Chem. Rev.* **2019**, *378*, 237.
- [29] A. Kochem, T. Weyhermüller, F. Neese, M. von Gastel, *Organometallics* **2015**, *34*, 995.
- [30] A. Ostericher, K. M. Waldie, C. P. Kubiak, *ACS Catal.* **2018**, *8*, 9596.
- [31] S. Fukuzumi, Y. M. Lee, W. Nam, *Coord. Chem. Rev.* **2018**, *355*, 54.

- [32] X. F. Liu, R. X. Li, X. T. Ren, Y. B. Yin, S. K. Mei, T. Liu, J. Yan, *J. Catal.* **2017**, *348*, 314.
- [33] L. Gan, T. L. Groy, P. Tarakeshwar, S. K. Mazinani, J. Shearer, V. Mujica, A. K. Jones, *J. Am. Chem. Soc.* **2015**, *137*, 1109.
- [34] Z. H. Pan, Y. W. Tao, Q. F. He, Q. Y. Wu, L. P. Cheng, Z. H. Wei, J. H. Wu, J. Q. Lin, D. Sun, Q. C. Zhang, D. Tian, G. G. Luo, *Chem-Eur. J.* **2018**, *24*, 8275.
- [35] B. D. McCarthy, C. L. Donley, J. L. Dempsey, *Chem. Sci.* **2015**, *6*, 2827.
- [36] L. C. Song, J. P. Li, Z. J. Xie, H. B. Song, *Inorg. Chem.* **2013**, *52*, 11618.
- [37] P. H. Zhao, Z. Y. Ma, M. Y. Hu, J. He, Y. Z. Wang, X. B. Jing, H. Y. Chen, Z. Wang, Y. L. Li, *Organometallics* **2018**, *37*, 1280.
- [38] I. Stamatopoulos, M. Roulia, K. A. Vallianatou, C. P. Raptopoulou, V. Psycharis, M. Carravetta, C. Papachristodoulou, E. Hey-Hawkins, I. D. Kostas, P. Kyritsis, *ChemistrySelect* **2017**, *2*, 12051.
- [39] S. M. Mansell, *Dalton Trans.* **2017**, *46*, 15157.
- [40] C. L. Deng, D. L. Zhang, B. Xie, C. Lai, L. X. He, S. P. Hu, Y. L. Li, Y. Wu, J. S. Feng, L. K. Zou, W. Y. Mou, J. Wei, *Polyhedron* **2018**, *155*, 407.
- [41] A. E. Pullen, R. M. Olk, *Coord. Chem. Rev.* **1999**, *188*, 211.
- [42] X. R. Chen, C. Xue, S. X. Liu, B. Cai, J. Wang, J. Q. Tao, Y. S. Xue, X. C. Huang, X. M. Ren, J. L. Liu, *Polyhedron* **2017**, *132*, 12.
- [43] X. R. Chen, X. Y. Xu, X. C. Huang, F. F. Ren, J. Wang, S. X. Liu, C. Xue, J. Q. Tao, *Polyhedron* **2018**, *147*, 55.
- [44] K. Ichihashi, D. Konno, T. Date, T. Nishimura, T. Nishimura, K. Y. Maryunina, K. Inoue, T. Nakaya, K. Toyoda, Y. Tatewaki, T. Akutagawa, T. Nakamura, S. Nishihara, *Chem. Mater.* **2018**, *30*, 7130.
- [45] C. X. Martins, G. B. Ferreira, R. A. Howie, J. Bordinhão, N. M. Comerlato, J. L. Wardell, S. M. S. V. Wardell, *Inorg. Chim. Acta* **2015**, *429*, 189.
- [46] Y. L. Li, L. K. Zou, B. Xie, X. Lin, S. S. Zhu, *Z. Anorg. Allg. Chem.* **2013**, *639*, 1787.
- [47] Y. F. Miura, M. Horikiri, S. H. Saito, M. Sugi, *Solid State Commun.* **2000**, *113*, 603.
- [48] P. H. Picciani, F. J. Pavinatto, N. M. Comerlato, G. Coutinho, O. N. Oliveira, *RSC Adv.* **2012**, *2*, 12835.
- [49] H. Jeon, W. Suh, D. Y. Noh, *Inorg. Chem. Commun.* **2012**, *24*, 181.
- [50] S. Jeon, W. Suh, D. Y. Noh, *Inorg. Chem. Commun.* **2017**, *81*, 43.
- [51] Z. R. Sun, M. H. Tong, H. P. Zeng, L. G. Ding, Z. G. Wang, Z. Z. Xu, J. Dai, G. Q. Bian, *Chem. Phys. Lett.* **2001**, *342*, 323.
- [52] P. Aloukos, S. Couris, J. B. Koutselas, G. C. Anyfantis, G. C. Papavassiliou, *Chem. Phys. Lett.* **2006**, *428*, 109.
- [53] L. T. Jin, X. Q. Wang, Q. Ren, N. N. Cai, J. W. Chen, T. B. Li, X. T. Liu, L. N. Wang, G. H. Zhang, L. Y. Zhu, D. Xu, *J. Cryst. Growth* **2012**, *356*, 10.
- [54] T. Kusamoto, H. Nishihara, *Coord. Chem. Rev.* **2019**, *380*, 419.
- [55] B. H. Solis, S. Hammes-Schiffe, *J. Am. Chem. Soc.* **2012**, *134*, 15253.
- [56] W. R. McNamara, Z. Han, C.-J. Yin, W. W. Brennessel, P. L. Holland, R. Eisenberg, *P. Natl. Acad. Sci.* **2012**, *109*, 15594.
- [57] A. Zarkadoulas, M. J. Field, V. Artero, C. A. Mitsopoulou, *ChemCatChem* **2017**, *9*, 2308.
- [58] C. N. Lin, D. Xue, Y. H. Zhou, S. Z. Zhan, C. L. Ni, *J. Electroanal. Chem.* **2017**, *785*, 58.
- [59] X. Ma, B. Xie, Y. L. Li, C. L. Deng, J. S. Feng, J. Wei, C. La, L. K. Zou, Y. Wu, J. Wang, L. X. He, D. L. Zhang, *Polyhedron* **2018**, *141*, 52.
- [60] A. Ghisolfi, C. Fliedel, V. Monakhov, K. Y. Monakhov, P. Braunstein, *Organometallics* **2014**, *33*, 2523.
- [61] X. F. Liu, *Inorg. Chim. Acta* **2014**, *421*, 10.
- [62] J. H. Aupers, Z. H. Chohan, N. M. Comerlato, R. A. Howie, A. C. Silvino, J. L. Wardell, S. M. S. V. Wardell, *Polyhedron* **2002**, *21*, 2107.
- [63] N. M. Comerlato, G. B. Ferreira, R. A. Howie, C. X. A. Silva, J. L. Wardell, *J. Organomet. Chem.* **2008**, *693*, 2424.
- [64] M. C. Burla, R. Caliandro, M. Camalli, B. Carrozzini, G. L. Cascarano, L. De Caro, C. Giacovazzo, G. Polidori, D. Siliqi, R. Spagna, *J. Appl. Cryst.* **2007**, *40*, 609.
- [65] G. M. Scheldrick, *Acta Crystallogr. C* **2015**, *71*, 3.
- [66] O. V. Dolomanov, L. J. Bourhis, R. J. Gildea, J. A. K. Howard, H. Puschmann, *J. Appl. Cryst.* **2009**, *42*, 339.
- [67] M. J. Frisch, G. W. Trucks, H. B. Schlegel, G. E. Scuseria, M. A. Robb, J. R. Cheeseman, G. Scalmani, V. Barone, B. Mennucci, G. A. Petersson, H. Nakatsuji, M. Caricato, X. Li, H. P. Hratchian, A. F. Izmaylov, J. Bloino, G. Zheng, J. L. Sonnenberg, M. Hada, M. Ehara, K. Toyota, R. Fukuda, J. Hasegawa, M. Ishida, T. Nakajima, Y. Honda, O. Kitao, H. Nakai, T. Vreven, J. A. Montgomery, Jr., J. E. Peralta, F. Ogliaro, M. Bearpark, J. J. Heyd, E. Brothers, K. N. Kudin, V. N. Staroverov, T. Keith, R. Kobayashi, J. Normand, K. Raghavachari, A. Rendell, J. C. Burant, S. S. Iyengar, J. Tomasi, M. Cossi, N. Rega, J. M. Millam, M. Klene, J. E. Knox, J. B. Cross, V. Bakken, C. Adamo, J. Jaramillo, R. Gomperts, R. E. Stratmann, O. Yazyev, A. J. Austin, R. Cammi, C. Pomelli, J. W. Ochterski, R. L. Martin, K. Morokuma, V. G. Zakrzewski, G. A. Voth, P. Salvador, J. J. Dannenberg, S. Dapprich, A. D. Daniels, O. Farkas, J. B. Foresman, J. V. Ortiz, J. Cioslowski, D. J. Fox, *Gaussian, Inc.*, Wallingford CT **2013**.
- [68] A. D. Becke, *J. Chem. Phys.* **1993**, *98*, 1372.
- [69] C. Lee, W. Yang, R. G. Parr, *Phys. Rev. B* **1988**, *37*, 785.
- [70] M. W. Wong, P. M. W. Gill, R. H. Nobes, L. Radom, *J. Phys. Chem.* **1988**, *92*, 4875.
- [71] A. G. B. da Cruz, J. L. Wardell, A. M. Rocco, *Thermochim. Acta* **2006**, *443*, 217.
- [72] X. Lin, B. Xie, L. K. Zou, Y. L. Li, X. L. Zhang, N. Zeng, *Phosphorus, Sulfur Silicon Relat. Elem.* **2015**, *190*, 1443.
- [73] A. N. Gupta, V. Kumar, V. Singh, K. K. Manar, A. K. Singh, M. G. B. Drew, N. Singh, *Inorg. Chim. Acta* **2013**, *408*, 145.
- [74] G. Soras, N. Psaroudakis, M. J. Manos, A. J. Tasiopoulos, D. G. Liakos, G. A. Mousdis, *Polyhedron* **2013**, *62*, 208.
- [75] X. F. Liu, X. Li, J. Yan, *Polyhedron* **2015**, *85*, 482.
- [76] A. D. Wilson, R. H. Newell, M. J. McNevin, J. T. Muckerman, M. R. DuBois, D. L. DuBois, *J. Am. Chem. Soc.* **2006**, *128*, 358.
- [77] R. Jain, A. A. Mamun, R. M. Buchanan, P. M. Kozlowski, C. A. Grapperhaus, *Inorg. Chem.* **2018**, *57*, 13486.
- [78] W. Y. Mou, T. Li, B. Xie, D. L. Zhang, C. Lai, C. L. Deng, J. X. Cao, X. X. Bai, X. Q. Liu, *Inorg. Chim. Acta* **2020**, *507*, 119587. <https://doi.org/10.1016/j.ica.2020.119587>
- [79] A. Z. Haddad, S. P. Cronin, M. S. Mashuta, R. M. Buchanan, C. A. Grapperhaus, *Inorg. Chem.* **2017**, *56*, 11254.

- [80] Y. L. Li, Z. Y. Ma, J. He, M. Y. Hu, P. H. Zhao, *J. Organomet. Chem.* **2017**, 851, 14.
- [81] V. Fourmond, P. A. Jacques, M. Fontecave, V. Artero, *Inorg. Chem.* **2010**, 49, 10338.
- [82] C. Costentin, H. Dridi, J.-M. Savéant, *J. Am. Chem. Soc.* **2014**, 136, 13727.

SUPPORTING INFORMATION

Additional supporting information may be found online in the Supporting Information section at the end of this article.

How to cite this article: Li T, Xie B, Cao J-X, et al. Heteroleptic dmit nickel complexes with bis (diphenylphosphanyl)amine ligands as robust molecular electrocatalysts for hydrogen evolution. *Appl Organomet Chem.* 2021;35:e6123. <https://doi.org/10.1002/aoc.6123>